Short Papers

A Compact Hall-Effect-Sensing 6-DOF Precision Positioner

Ho Yu and Won-jong Kim

***Abstract*—This paper presents the design, control, and implementation of a compact high-precision multidimensional positioner. A 1.52-kg single levitated moving part, named as the platen, generates all six-axis fine and coarse motions, resulting in a reliable and effective positioning system. Three laser distance sensors are used to measure its vertical translational motion and x- and y-axis rotational motion. Three two-axis Hall-effect sensors are used to determine its lateral motions and rotational motion about the z-axis by measuring the magnetic flux density generated by a magnet matrix. Real-time control is implemented on a Linux-based operating system, Real-Time Application Interface (RTAI) with COntrol and MEasurement Device Interface (Comedi) and Comedi libraries. A maximum travel of 220 mm in the x-direction and 200 mm in the y-direction, and a rotation angle of 18.6° about the z-axis were achieved experimentally. A maximum velocity of 0.3 m/s with an acceleration of 3.6 m/s^2 was obtained in the y-direction. Step responses the demonstrated a 10-μm resolution and 6-μm rms noise in the translational mode. This compact single-moving-part positioner is suitable for use in precision-positioning systems, e.g., in semiconductor manufacturing.**

***Index Terms*—Hall-effect sensor, precision manufacturing, precision positioning, real-time digital control, Real-Time Application Interface (RTAI).**

I. Introduction

In modern nanoscale and microscale engineering applications, such as wafer steppers in semiconductor manufacturing, high-precision motion control is a key component. The motion profile of wafer steppers requires not only high resolution and precision, but also multidimensional motion with a large travel range and high control bandwidth [1]–[4]. A planar motor is a good candidate as an actuator for a precision-positioning stage. The advantage of a planar motor is multidimensional motion with a large travel range that can be provided with high precision. The Sawyer motor is one of the first planar motors commercialized by Northern Magnetics and Megamation [5]–[7]. It exhibited a two-phase full-step motion as coarse as 250 μm with a positioning repeatability of the order of 5 μm. The Sawyer motor requires a tight air gap of less than 25 μm; therefore, it should be operated with an ultrafine motor surface finish with precisely manufactured teeth. Other drawbacks of the sawyer motor include a large attractive force of 1800 N, large cogging force, and overheating.

The compact multidimensional precision-positioning stage presented in this paper uses a stator of a superimposed Halbach magnet matrix and a synchronous permanent magnet planar motor [3], [8]. The earlier positioner in our laboratory was capable of generating 6-DOF

Manuscript received September 16, 2009; revised February 12, 2010 and April 23, 2010; accepted April 30, 2010. Date of publication June 3, 2010; date of current version December 15, 2010. Recommended by Technical Editor G. Yang. This work was supported in part by the Texas Advanced Technology Program under Grant 000512-0225-2001.

H. Yu is with the Pohang Iron and Steel Company Technical Research Laboratories, Pohang, 790-300, Korea (e-mail: jameskaten@gmail.com; jameskaten@posco.com).

W. Kim is with the Department of Mechanical Engineering, Texas A&M University, College Station, TX 77843-3123 USA (e-mail: wjkim@tamu.edu).

Color versions of one or more of the figures in this paper are available online at http://ieeexplore.ieee.org.

Digital Object Identifier 10.1109/TMECH.2010.2050003

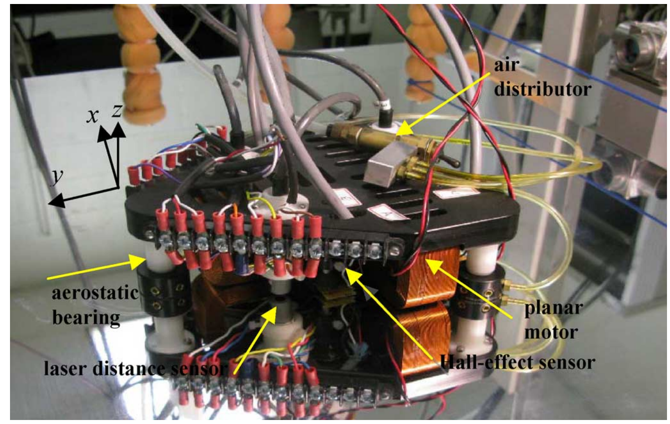

Fig. 1. Photograph of the precision positioner.

motions with a 20-nm positioning noise using laser interferometers [2]. A laser interferometer is a prevailing sensor in positioning devices that require high precision. However, it has several drawbacks such as high cost, complicated alignment, and limited rotational sensing. On the other hand, a two-axis Hall-effect sensor is not only cost-effective, but also capable of measuring large rotational motion with good resolution [9], [10]. The precision positioner presented in this paper uses three two-axis Hall-effect sensors to measure lateral motion in the x- and y-directions, and rotation about the z-axis with the positioning resolution of the order of micrometers.

Section II presents the positioner design concept, and Section III illustrates the working principles of the two-axis Hall-effect sensors. Sections IV and V present the dynamic analysis and real-time control of the positioner supported by experimental results.

II. Compact 6-DOF Precision Positioner

The design objectives of this positioner are the minimization of platen mass, enhancement of dynamic performance, extension of planar motion, and low cost. Fig. 1 shows a photograph of the compact multidimensional positioner [3]. The overall dimension of the platen is 170.18 mm × 152.40 mm × 53.34 mm. The single moving frame, named as the platen, can generate 6-DOF fine and coarse motions. For the lateral motion measurement, three two-axis Hall-effect sensors are used instead of laser interferometers. They can also have unlimited travel range in translational motions. The platen is the single moving part, comprising a main body made of Delrin with the mass density of 1.54 g/cm^3, three-phase planar motor armatures, three aerostatic bearings, three laser distance sensors for vertical motion sensing, three two-axis Hall-effect sensors for lateral motion sensing, and two terminal blocks for wire connection. Three two-axis Hall-effect sensors are used in part because they have unlimited travel ranges in translation motions.

This moving-coil platen has two key advantages: 1) the entire system is lightweight so that the platen can generate faster dynamics and consume less power; 2) by extending the permanent magnet matrix, the maximum travel range can be easily extended. In addition, this positioner has additional advantages to be used as a semiconductor-manufacturing positioning stage. A mechanically noncontact frame produces no wear particles and is compatible with the clean-room

TABLE I
PARAMETERS OF THE PLANAR MOTOR ARMATURES AND THE MAGNET MATRIX

Specifications	Values
Number of motor picth	$N_m = 1/2$
Pitch, l	50.977 mm = 2.007 in
Winding thickness, Γ	$l/5$
Turn density, η_0	3.5246×10^6 turns/m²
Nominal peak current density	2×10^6 A/m²
Magnet array width, w	12.7 mm
Nominal motor air gap, z_0	2.3 mm
Magnet matrix size	304.8 × 304.8 mm
Magnet thickness, Δ	$l/4$
Equivalent magnet remanence	$\mu_0 M_0 = 0.71$ T
Fundamental wave number	$\gamma_1 = 2\pi/l = 123.25$ m^{-1}

TABLE II
SPECIFICATIONS OF THE 2D-VD-11SO TWO-AXIS HALL-EFFECT SENSOR [10]

Specifications	Conditions	Values
Input resistance	$B = 0$ mT, $I_c = 2$ mA	2.2 kΩ
Output resistance	$B = 0$ mT, $I_c = 2$ mA	8.5 kΩ
Output voltage	Constant current drive $B = 1$ T, $I_c = 2$ mA	400 mV
Offset voltage	$B = 0$ mT, $I_c = 2$ mA	± 3 mV
Sensitivity	$I_c = 2$ mA	400 mV/T
Resolution		2 μT
Magnetic sensitive volume		0.25 × 0.25 × 0.20 mm

environment. A single rigid moving frame can have high natural frequencies; therefore, faster dynamics with high reliability and low power consumption in multidimensional positioning can be obtained.

The superimposition of two orthogonal Halbach magnet arrays on the base plate produces a concentrated-field magnet matrix [4]. The magnet matrix consists of six pitches in the x- and y-directions, respectively. Four magnet blocks form one sinusoidal cycle that is called a pitch. Table I presents key motor and magnet-matrix parameters.

III. TWO-AXIS HALL-EFFECT SENSORS AND THEIR OPERATION

Three two-axis Hall-effect sensors are used for lateral position measurements. Specifications of the Hall-effect sensor are presented in Table II. Each Hall-effect sensor has two orthogonal axes and measures the magnetic flux density in two independent perpendicular axes. A single Hall-effect sensor cannot detect the unique position of the platen, because there are two of the equal magnitude points in a one-pitch sinusoidal magnetic flux density. Therefore, two Hall-effect sensors collaborate to measure one-axis motion. Moreover, the phase difference between the two Hall-effect sensors is used to determine the direction of motion. The magnetic flux density exhibits symmetry and periodicity with a sensor position gap

$$\left(\frac{1}{4}+\frac{1}{2}n\right)\times\text{pitch},\qquad n = 1,\ 2,\ 3,\ \ldots. \tag{1}$$

Fig. 2 shows a top view of the platen to illustrate the geometrical relations of the three Hall-effect sensors. One of the two adjacent sensors (the set of sensors A and B and the set of sensors A and C) is always located in one of the sensitive intervals drawn by thick lines in Fig. 3, where the gradient of magnetic flux density is large with respect

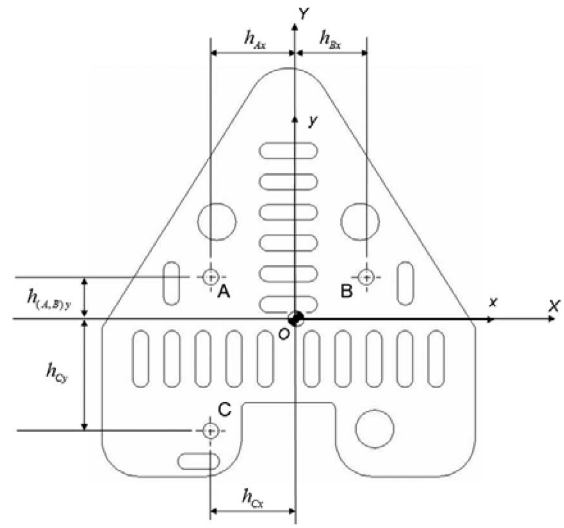

Fig. 2. Locations of the three Hall-effect sensors. The numerical values of the parameters are $h_{Ax} = 33.57$ mm, $h_{Bx} = 30.81$ mm, $h_{Cx} = 33.47$ mm, $h_{Ay} = 13.77$ mm, $h_{By} = 13.77$ mm, and $h_{Cy} = 49.73$ mm.

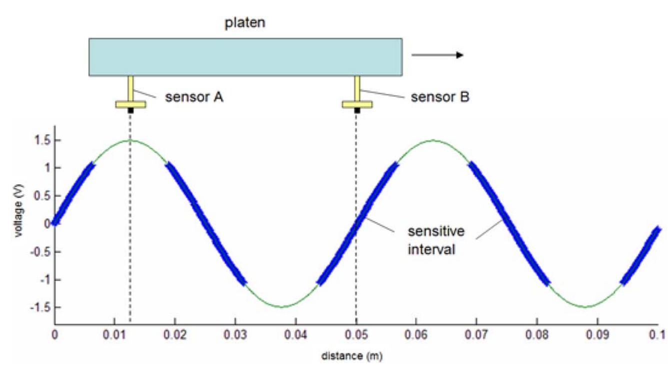

Fig. 3. Illustration of the sensor switching and collaboration principle. Sensor B is in one of the sensitive intervals.

to the position. The periodic magnetic flux density is converted to a voltage signal.

Since we use the sensitive intervals, a sensor switching is required at every quarter pitch. This sensor switching takes place repeatedly as the platen moves over multiple pitches.

Four voltage readings V_{ax}, V_{bx}, V_{ay}, and V_{cy} are used to determine the platen translations in the x- and y-axes. Voltage data directly from the Hall-effect sensors need to be normalized with the same magnitudes for accurate position measurement. With the calibration constants of ω_{ax}, ω_{bx}, ω_{ay}, and ω_{cy} and the offset values of $V_{ax\text{offset}}$, $V_{bx\text{offset}}$, $V_{ay\text{offset}}$, and $V_{cy\text{offset}}$, the values of a_x, b_x, a_y, and c_y in (2)–(5) represent the normalized sensor data

$$a_x = \sin(\omega_{ax}V_{ax} + V_{ax\text{offset}}) \tag{2}$$

$$b_x = \sin(\omega_{bx}V_{bx} + V_{bx\text{offset}}) \tag{3}$$

$$a_y = \sin(\omega_{ay}V_{ay} + V_{ay\text{offset}}) \tag{4}$$

$$c_y = \sin(\omega_{cy}V_{cy} + V_{cy\text{offset}}). \tag{5}$$

A pitch of the magnetic flux density wave consists of eight distinct sections that are adopted with different calibration factors. These eight sections are repeated over the entire magnet matrix due to the periodicity of the magnetic flux density. For example, in the first section, the sensitive interval of sensor A is used with a scaling factor of α in the x- and y-directions. Sensor data Δx_b in the x-axis and Δy_c in the y-axis compensate for the variables of Δx_d and Δy_d; the final position displacement of the platen in the x- and y-directions with a scaling factor of β

$$\Delta x_d = \alpha \cdot \Delta x_a + \beta \cdot \Delta x_b \tag{6}$$

$$\Delta y_d = \alpha \cdot \Delta y_a + \beta \cdot \Delta y_c \tag{7}$$

where Δx_a, Δx_b, Δy_a, and Δy_c are the derivative of a_x, b_x, a_y, and c_y, respectively. Hence, the sensors can measure unrestricted motion in the x–y plane with respect to the size of the magnet matrix.

Using this principle, the rotation about the z-axis can also be determined. Sensors A and B detect the distance at each location. The difference between the two sensor measurements in the y-axis is used in triangulation as follows:

$$\psi = \tan^{-1}\left(\frac{\Delta A - \Delta B}{\overline{AB}}\right) \tag{8}$$

where $\overline{AB}$ is the lateral distance between sensors A and B, which is 63.5 mm.

IV. Dynamic Modeling and Controller Design

The decoupled forces in both the horizontal and vertical directions are derived as follows:

$$\begin{bmatrix} f_y \\ f_z \end{bmatrix} = \frac{1}{2}\mu_0 M_0 \eta_0 N_m G e^{-\gamma_1 z_0} \begin{bmatrix} \cos\gamma_1 y & \sin\gamma_1 y \\ -\sin\gamma_1 y & \cos\gamma_1 y \end{bmatrix} \times \begin{bmatrix} \frac{2}{3} & -\frac{1}{3} & -\frac{1}{3} \\ 0 & \frac{1}{\sqrt{3}} & -\frac{1}{\sqrt{3}} \end{bmatrix} \begin{bmatrix} i_A \\ i_B \\ i_C \end{bmatrix} \tag{9}$$

where the motor geometric constant G is 1.072×10^{-5} m^3. [2]

The equations of motion based on Newton's second law in the horizontal plane are as follows:

$$M\frac{d^2(x,y)}{dt^2} = f_{(x,y)} \qquad I_{zz}\frac{d^2\psi}{dt^2} = M_{oz}. \tag{10}$$

The dynamic models for vertical modes are as follows:

$$M\frac{d^2 z}{dt^2} = f_z - K_z z \tag{11}$$

$$I_{xx}\frac{d^2\theta}{dt^2} = M_{ox} - K_\theta \theta \qquad I_{yy}\frac{d^2\varphi}{dt^2} = M_{oy} - K_\varphi \varphi \tag{12}$$

where M is the total platen mass of 1.52 kg. The principal moments of inertia of I_{xx}, I_{yy}, and I_{zz} are 0.0037, 0.0019, and 0.0022 kg·m^2, respectively. The effective spring constant of the motor is $K_z = 620$ N/m, which is determined by experiments based on Hooke's law. K_θ and K_φ are the effective torsional spring constants, which are determined experimentally as 65 and 87 N·m·rad^{-1}, respectively.

Second-order digital lead-lag controllers were designed with the dynamic models in all axes, as given in (13). The sampling frequency of 1 kHz was selected

$$G_{x,y}(z) = 1.51 \times 10^5 \left(\frac{z - 0.9673}{z - 0.3433}\right)\left(\frac{z - 0.9901}{z - 1}\right). \tag{13}$$

The controller of the rotation about the z-axis has a gain of 1.87×10^3. The crossover frequencies in the horizontal modes are 25.27 and 22.4 Hz with the phase margins of 73.1° and 66.3°, respectively. Similarly, the vertical-mode controllers were designed as follows:

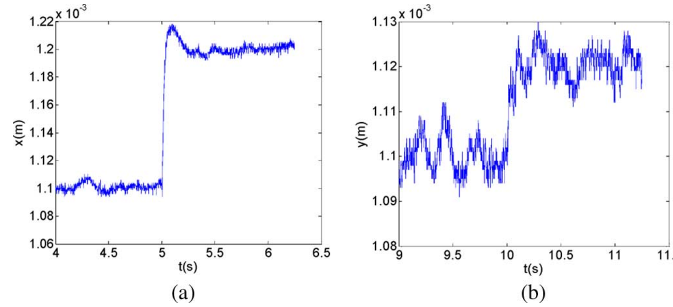

Fig. 4. (a) 100-μm step response in the x-direction. (b) 20-μm step response in the y-direction.

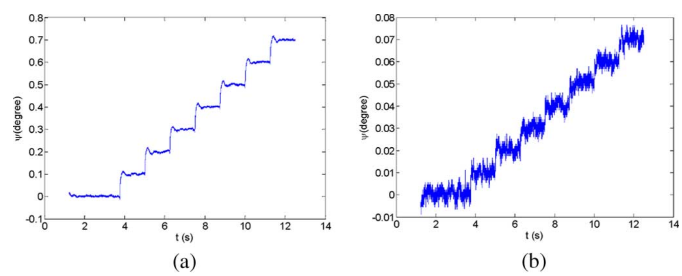

Fig. 5. (a) 0.1° and (b) 0.01° rotational motions about the z-axis.

$$G_z(z) = 298600\left(\frac{z - 0.879}{z - 0.379}\right)\left(\frac{z - 0.988}{z - 1}\right) \tag{14}$$

$$G_\theta(z) = 854\left(\frac{z - 0.905}{z - 0.470}\right)\left(\frac{z - 0.988}{z - 1}\right) \tag{15}$$

$$G_\varphi(z) = 1020\left(\frac{z - 0.905}{z - 0.470}\right)\left(\frac{z - 0.988}{z - 1}\right). \tag{16}$$

Pure integrators located at $z = 1$ eliminate the steady-state error introduced by the aerostatic bearings and the umbilical cables.

V. Real-Time Control Experimental Results

Ubuntu with RTAI has been installed and demonstrated with the user interface for our real-time control system. RTAI is a kernel-modified package of Linux. A standard Linux kernel and RTAI can be used with Comedi and libraries.

The real-time control system acquires analog data from the sensors through an A/D converter board (NI-6221). A Pentium IV PC compiles the C codes that include the real-time control and digital signal processing routines. The position command data computed from the PC flow to the D/A converters on NI-6703, which supports sixteen 16-bit analog output voltage channels with a $\pm$10 V voltage swing and 8 digital I/O lines.

A 100-μm step response in the x-direction and a 20-μm step response in the y-direction are presented in Fig. 4. The results demonstrate a rise time of less than 25 ms, a maximum overshoot of about 20%, and a settling time of less than 220 ms without any steady-state errors in the x- and y-axes. The resolution is better than 10 μm and the position noise is 6 μm rms in both the x- and y-axes. The position noise is mainly caused by the Hall-effect sensors' electronics and the unsteady airflow through the aerostatic bearings. Staircase step responses of 0.1° and 0.01° rotations about the z-axis are presented in Fig. 5.

Long-range planar motions are commonly required in precision-positioning applications, such as scanning and microlithography. One

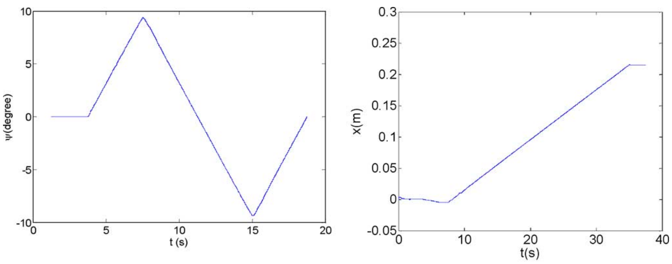

(a) (b)

Fig. 6. (a) 18.6° rotational motion in the z-axis and (b) maximum travel range of 220 mm in the x-direction.

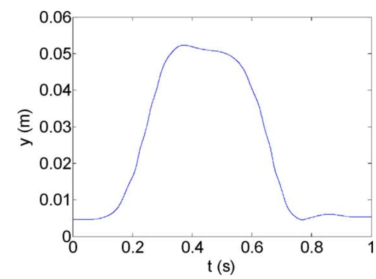

Fig. 7. Position profile in the y-axis with respect to time.

of the key advantages of this positioning stage is that the angular measurement range with the Hall-effect sensors is much larger than that of laser interferometers. Fig. 6(a) presents the large-angle rotation motion of 18.6°. The maximum travel range of the positioner in the x-axis is presented in Fig. 6(b). The travel ranges of 220 mm in the x-direction and 200 mm in the y-direction were achieved in the x–y plane. The scanning velocity was 8 mm/s.

A position profile is one of the important features in precision positioning. This compact multidimensional positioner is currently capable of generating a maximum velocity of 0.3 m/s in the y-direction. Fig. 7 illustrates that a maximum velocity of 0.3 m/s was achieved between 0.2 s and 0.3 s with an acceleration of 3.6 m/s^2. Less than 5% overshoot due to the abrupt velocity change occurred at the ends of the steps.

VI. Conclusion

In this paper, a compact multidimensional precision positioner was developed and implemented. Three planar motors on the bottom of the platen can generate 6-DOF motions. Three two-axis Hall-effect sensors measure translational motions and three laser distance sensors are involved in measuring vertical displacements. The positioner was controlled by a Linux-based real-time system, and digital lead-lag compensators were designed at 1 kHz sampling frequency.

Unrestricted translations and large rotational angles based on the size of the magnet matrix are one of the key advantages of the two-axis Hall-effect sensors used in this research. A compact size and minimized mass of the platen exhibits excellent dynamics. In addition, a Linux real-time system on a PC costs much less than a DSP-based control units with laser interferometers. This compact 6-DOF positioner has potential applications in the precision-positioning industry.

Acknowledgment

The authors would like to thank T. Hu, N. Bhat, Y. Kawato, and A. Ambike, former graduate students of W.-J. Kim, for their contributions to this project.

References

[1] Y. Li and Q. Xu, "Development and assessment of a novel decoupled XY parallel micropositioning platform," *IEEE/ASME Trans. Mechatronics*, vol. 15, no. 1, pp. 125–135, Feb. 2010.
[2] T. Hu and W.-J. Kim, "Extended-range 6-DOF high-precision positioner for wafer processing," *IEEE/ASME Trans. Mechatronics*, vol. 11, no. 6, pp. 682–689, Dec. 2006.
[3] H. Yu, "Design and control of a compact 6-degree-of-freedom precision positioner with linux-based real-time control," Ph.D. dissertation, Dept. Mech. Eng., Texas A&M Univ., College Station, TX, Aug. 2009.
[4] W.-J. Kim, "High-precision planar magnetic levitation," Ph.D. dissertation, Massachusetts Inst. Technol., Cambridge, MA, 1997.
[5] B. A. Sawyer, "Magnetic positioning device," U.S. Patent 3 376 578, Apr. 2, 1968.
[6] Megamation. (2010). [Online]. Available: http://www.megamation.com
[7] Normag, *Northern Magnetics Linear Motor Technology Manual*, Northern Magnetics Inc., Santa Clarita, CA, 1998.
[8] N. Fujii and T. Kihara, "Surface induction motor for two-dimensional drive," *Elect. Eng. Jpn.*, vol. 130, no. 4, pp. 107–115, Jan. 2000.
[9] Y. Kawato and W.-J. Kim, "Multi-degree-of-freedom precision position sensing and motion control using two-axis Hall-effect sensors," *Trans. ASME, J. Dyn. Syst., Meas., Control*, vol. 128, no. 4, pp. 980–988, Dec. 2006.
[10] Hall-effect sensor. (2010). [Online]. Available: http://www.sentron.ch

Analysis of Pole Configurations of Permanent-Magnet Spherical Actuators

Liang Yan, I-Ming Chen, Hungsun Son, Chee Kian Lim, and Guilin Yang

***Abstract*—This paper presents a generic design concept of three degree-of-freedom (3-DOF) permanent-magnet (PM) spherical actuators. A ball-shaped rotor mounted with multiple layers of PM poles is concentrically housed in a spherical-shell-like stator with multiple layers of air-core coils. This design allows more rotor and stator poles to be incorporated to increase torque output and motion range of the actuator. The magnetic field and torque modeling methods are generalized to multiple layers of poles, which provides a convenient way to analyze field distribution and torque performance of spherical actuators with various pole configurations. The simulation results of flux distribution and torque variation of double-layer configuration are compared with those of single-layer one. It shows that the magnetic field distribution and torque variation for both configurations are coincident with PM-pole arrangement on the rotor surface. The tilting torque of double-layer design is larger than that of single layer, and the torque variation is more uniform. The spinning torque of single layer is relatively large. The proposed analyzing methods of field and torque could be employed for preliminary study of other PM spherical actuators.**

***Index Terms*—Magnetic field, spherical actuator, torque.**

Manuscript received September 2, 2008; revised November 19, 2008 and March 13, 2009; accepted March 22, 2009. Date of publication July 1, 2010; date of current version December 15, 2010. Recommended by Technical Editor M. Benbouzid. This work was supported by the Fundamental Research Funds for the Central Universities.

L. Yan is with the School of Automation Science and Electrical Engineering, Beihang University, Beijing 100191, China (e-mail: yanliang@pmail.ntu.edu.sg).

I.-M. Chen, H. Son, and C.-K. Lim are with the School of Mechanical and Aerospace Engineering, Nanyang Technological University, Singapore 639798 (e-mail: michen@ntu.edu.sg; hsson@ntu.edu.sg; CKLim@ntu.edu.sg).

G. Yang is with Mechatronics Group, Singapore Institute of Manufacturing Technology, Singapore 638075 (e-mail: glyang@simtech.a-star.edu.sg).

Color versions of one or more of the figures in this paper are available online at http://ieeexplore.ieee.org.

Digital Object Identifier 10.1109/TMECH.2010.2051160